A temperature-variant method for performance modeling and economic analysis of thermoelectric generators: Linking material properties to real-world conditions

Naman S. Benday [a], Daniel M. Dryden [b], Kurt Kornbluth [c], Pieter Stroeve [a],*

[a] Department of Chemical Engineering, University of California Davis, Davis, CA 95616, USA
[b] Department of Materials Science and Engineering, University of California Davis, Davis, CA 95616, USA
[c] Department of Mechanical and Aerospace Engineering, University of California Davis, Davis, CA 95616, USA

HIGHLIGHTS

- A numerical method predicts power and financial costs of a thermoelectric generator.
- Temperature-dependent, experimental materials properties and variable heat sources are used.
- Sensitivity analyses show improvements can be made by choosing higher temperature heat sources.
- Optimizing the choice of heat exchanger lowers cost.
- A higher figure of merit improves performance and lowers cost.

ARTICLE INFO

ABSTRACT

A new methodology for the systematic study of thermoelectric generator (TEG) design and economic analysis is presented, with the objective of assessing the performance and financial feasibility of small-scale TEG installations, for 4 leading candidate thermoelectric materials. Temperature of a steam trap pipe surface were measured at the University of California Davis Pilot Brewery, and device performance was modeled using the finite-element modeling software ANSYS. The model integrated temperature-dependent material properties from leading candidate thermoelectric materials and experimental time-variant temperature data. Calculated power outputs were utilized in a net present value (NPV) framework to assess the financial feasibility and economic implications of small scale TEG installations, as well as to address the aspects of TEG research, design and implementation which have potential for rapid and substantive improvement. This model, along with case study results, provides a powerful platform for analyzing the performance of real-world systems and can be used to predict where further technological development on TEG materials and devices would be most effective. It is found that a *BiSbTe* based TEG generated the highest power output at the measured temperatures and consequently resulted in the highest NPV at the end of 25 years. Sensitivity analysis of the NPV revealed a strong dependence on the heat-exchanger cost, highlighting the importance of efficient heat transfer design. The *zT* necessary for a 7-year payback period as a function of the capital cost and hot-side temperature was also calculated for a *SiGe* based TEG.

© 2016 Elsevier Ltd. All rights reserved.

1. Motivation

Thermoelectric installations can provide a source of green electricity, especially when in high-value on-site applications, but financial viability is highly sensitive to source temperature, device efficiency, maintenance cost, and projected device lifetime [1–4].

The integration of TEGs may also facilitate added functionality that would not be possible without their use: for instance, self-powered furnaces and co-generation systems [4–7] for use in remote regions, waste heat recovery from automobile exhausts [8,9], building-integrated power generation [10], and wearable electronics that may be powered indefinitely by harvesting body heat [11–13]. And a variety of other energy applications [14–18].

Recent studies for module-level TEG performance have assumed constant hot and cold-side temperatures, and operation

---

Nomenclature

ρ	density, $\frac{\text{kg}}{\text{m}^3}$		ε	dielectric permittivity matrix, $\frac{\text{F}}{\text{m}}$

ρ density, $\frac{\text{kg}}{\text{m}^3}$

C specific heat capacity, $\frac{\text{J}}{\text{kg·K}}$

T absolute temperature, K

$\dot{q}$ heat generation rate per unit volume, $\frac{\text{W}}{\text{m}^3}$

$\vec{q}$ heat flux vector, $\frac{\text{W}}{\text{m}^2}$

$\vec{J}$ electric current density vector, $\frac{\text{A}}{\text{m}^2}$

$\vec{E}$ electric field intensity vector, $\frac{\text{V}}{\text{m}^2}$

$\vec{D}$ electric flux density vector, $\frac{\text{C}}{\text{m}^2}$

λ thermal conductivity matrix, $\frac{\text{W}}{\text{m·K}}$

σ electrical conductivity matrix, $\frac{\text{S}}{\text{m}}$

α Seebeck coefficient matrix, $\frac{\text{V}}{\text{K}}$

$\Pi = T\boldsymbol{\alpha}$ Peltier coefficient matrix, V

ε dielectric permittivity matrix, $\frac{\text{F}}{\text{m}}$

Thermal stiffness matrix $\boldsymbol{K}^{TT} = \int \nabla \boldsymbol{N} \cdot [\lambda] \cdot \nabla \boldsymbol{N} dV$

Electric stiffness matrix $\boldsymbol{K}^{\varphi\varphi} = \int \nabla \boldsymbol{N} \cdot [\sigma] \cdot \nabla \boldsymbol{N} dV$

Seebeck stiffness matrix $\boldsymbol{K}^{\varphi T} = \int \nabla \boldsymbol{N} \cdot [\sigma] \cdot [\alpha] \cdot \nabla \boldsymbol{N} dV$

Thermal damping matrix $\boldsymbol{C}^{TT} = \rho \int C \boldsymbol{N} \boldsymbol{N} dV$

Dielectric damping matrix $\boldsymbol{C}^{\varphi\varphi} = \int \nabla \boldsymbol{N} \cdot [\varepsilon] \cdot \nabla \boldsymbol{N} dV$

Thermal stiffness matrix $\boldsymbol{K}^{TT} = \int \nabla \boldsymbol{N} \cdot [\lambda] \cdot \nabla \boldsymbol{N} dV$

$\vec{Q}$ vector of combined heat generation loads

Peltier heat load vector $\vec{Q}^P = \int \nabla \boldsymbol{N} \cdot [\Pi] \cdot \boldsymbol{J} dV$

Electric power load vector $\vec{Q}^e = \int \boldsymbol{N} \boldsymbol{E} \cdot \boldsymbol{J} dV$

under steady-state conditions [18–20]. However, many potential heat sources show significant temperature variation during the course of operation, and given the strong temperature dependence of all material properties that contribute to the thermoelectric figure of merit zT [19,21], understanding the temperature and time variance of the potential power generation of a particular TEG system is critical to accurately modeling its real-world performance. Previous financial analyses [1–3] while thorough and robust within the model conditions, do not account for temperature variation, and rely on similar approximations of device performance that may be refined with the inclusion of time- and temperature-variant device performance modeling. Financial forecasting and sensitivity studies indicate that TEG installations provide a feasible source of green electricity but are highly sensitive to source temperature, device efficiency, discount rate, and projected device lifetime.

This analysis integrates real-time hot side temperature data, gathered from the pilot brewery at the UC Davis August A. Busch III Brewing & Food Science Laboratory, with a model that was formulated using finite-element software ANSYS to accurately predict the expected power outputs from various thermoelectric materials given the hot side temperature conditions. Thermoelectric material properties are a function of temperature, and during operation there is a temperature gradient across the TEG device (Fig. 1). It is therefore important that a model take into consideration the variation in material properties along the length of a thermoelectric leg. The model used in this paper accounts for such variations caused by the temperature gradient and thus provides a more accurate prediction of the power output as compared to simplified analytical models that assume a constant temperature during operation [8,9]. The power output results are fed into an economic model that calculates the Net Present Value (NPV) of TEG installations given realistic cost and income parameters (See Methods). This methodology is generalizable to a range of different TEG materials, systems, and operating conditions, wherever the material properties are known and operating temperatures can be measured, and is especially useful in systems with widely varying input temperatures for which more simplistic models are not sufficiently powerful.

2. Theoretical background

Finite element modeling (FEM) has become an extremely valuable solution technique for coupled-field (for example, thermal-electric) analyses in many areas of engineering and physics. FEM is versatile in its applicability to arbitrarily shaped structures, complex materials, and various loads and boundary conditions. ANSYS, the FEM software used in this study, has a large library of elements that support structural, thermal, fluid, acoustic, and electromagnetic analyses [22]. Below is a brief summary of the equations of thermal-electric analysis utilized by ANSYS [22].

The equation for heat flow in thermoelectric analysis is:

$$\rho C \frac{\partial T}{\partial t} + \nabla \cdot \vec{q} = \dot{q} \tag{1}$$

And of continuity of electric charge:

$$\nabla \cdot \left(\vec{J} + \frac{\partial \vec{D}}{\partial t} \right) = 0 \tag{2}$$

Those 2 equations are coupled by the following constitutive equations of thermoelectricity:

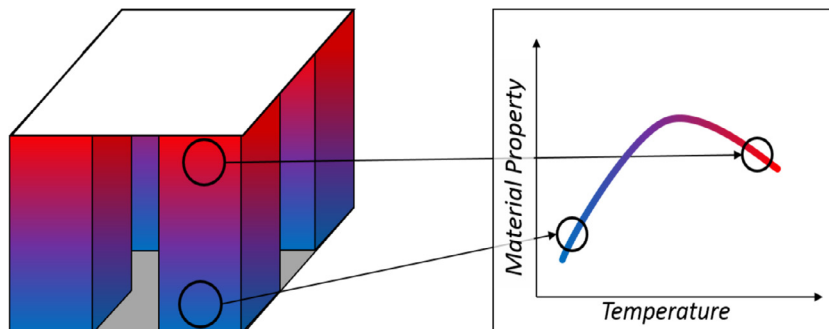$$\vec{q} = \Pi \cdot \vec{J} - \lambda \cdot \nabla T \tag{3}$$

Fig. 1. Schematic illustration of a multi-leg thermoelectric device (left) and how material properties, such as the Seebeck coefficient, may vary with temperature within a thermoelement leg.

$$\vec{J} = \boldsymbol{\sigma} \cdot (\vec{E} - \boldsymbol{\alpha} \cdot \nabla T) \tag{4}$$

And the constitutive equation for a dielectric medium is

$$\vec{D} = \boldsymbol{\varepsilon} \cdot \vec{E} \tag{5}$$

In the absence of a time-variant magnetic field, the electric field is given by:

$\vec{E} = -\nabla \varphi$, where φ is an electric potential scalar. The electric field E is irrotational, which means that $\nabla \times \vec{E} = 0$. Substituting the constitutive equations of thermoelectricity in the main equations (1) and (2) we obtain:

$$\rho C \frac{\partial T}{\partial t} + \nabla \cdot (\boldsymbol{\Pi} \cdot \vec{J}) - \nabla \cdot (\boldsymbol{\lambda} \cdot \nabla T) = \dot{q} \tag{6}$$

$$\nabla \cdot \left(\boldsymbol{\varepsilon} \cdot \nabla \frac{\partial \varphi}{\partial t} \right) + \nabla \cdot (\boldsymbol{\alpha} \cdot \boldsymbol{\sigma} \cdot \nabla T) - \nabla \cdot (\boldsymbol{\sigma} \cdot \nabla \varphi) = 0 \tag{7}$$

2.1. Finite element formulation

The coupled system of thermoelectric equations derived above can be modified into a system of thermoelectric finite element equations using the Galerkin FEM procedure [18]. This method involves:

(1) Approximating the temperature and electric scalar potential over a finite element as:

$$T = \vec{N} \cdot \vec{T_e}$$

$$\varphi = \vec{N} \cdot \vec{\varphi_e}$$

where: $\vec{N}$ = vector of finite element shape functions. $\vec{T_e}$ = vector of nodal temperatures. $\vec{\varphi_e}$ = vector of nodal electric potentials.
(2) Writing the system of equations derived above in their weak projective forms
(3) Integrating those equations by parts and applying Neumann boundary conditions

The resulting system of finite element equations can be written as:

$$\begin{bmatrix} \boldsymbol{C^{TT}} & 0 \\ 0 & \boldsymbol{C^{\varphi\varphi}} \end{bmatrix} \begin{pmatrix} \vec{T_e} \\ \vec{\varphi_e} \end{pmatrix} + \begin{bmatrix} \boldsymbol{K^{TT}} & 0 \\ \boldsymbol{K^{T\varphi}} & \boldsymbol{K^{\varphi\varphi}} \end{bmatrix} \begin{pmatrix} \vec{T_e} \\ \vec{\varphi_e} \end{pmatrix} = \begin{pmatrix} \vec{Q} + \vec{Q^P} + \vec{Q^e} \\ I \end{pmatrix} \tag{8}$$

Thermal loads can be input to the model in the form of a constant temperature boundary condition, heat flow rate boundary condition, heat flux boundary condition, convection, radiation, as well as heat generation rate boundary condition for a heat source. Electric loads can be imposed in form of an electric potential and point electric current [22]. Electric components like resistors and capacitors can be connected to the FEM model to simulate active and passive electrical loads. The material matrices are input into the model along their diagonal terms, or along the $x, y,$ and z axes. This can be combined with an arbitrarily oriented co-ordinate system to account for non-isotropic material properties. The material properties used in this study are all assumed to be isotropic.

The electrical properties are input in the form of resistivity, which ANSYS internally converts to the electrical conductivity $[\sigma]$ matrix, and the thermal properties are input as the thermal conductivity matrix $[\lambda]$ [3]. The material properties can be temperature-dependent and can be directly defined as functions of temperature. They can also be manually specified for different

temperatures from a plot. The Thomson effect is taken into consideration only if the Seebeck coefficients are specified to be temperature-dependent [22]. The analysis is supported by 3 coupled field elements:

(1) PLANE223
(2) SOLID226
(3) SOLID227

All of the above elements have electrical, thermal, and structural degrees of freedom at their nodes. The element SOLID 226 has been used in this analysis, and is a 3-dimensional 20-node hexahedron, which can be degenerated into a 10-node tetrahedron, a 13-node pyramid, or a 15-node prism [3]. The analysis is nonlinear because the thermal load vector is dependent on the electrical load vector, and therefore the analysis requires at least 2 iterations to converge. A solution is obtained by the ANSYS Mechanical APDL Solver using the Newton-Raphson method. The solution gives the temperature T_e and electric potential φ_e at unconstrained nodes, or nodes at which no boundary conditions have been imposed. The model also computes the heat flow at nodes where temperature and electric potential have been imposed. The temperature and voltage gradients are calculated as:

$$\nabla T = \nabla \boldsymbol{N} \cdot \boldsymbol{T_e}$$
$$\nabla \varphi = \nabla \boldsymbol{N} \cdot \boldsymbol{\varphi_e}$$

These are then substituted in equations to obtain $\boldsymbol{J}, \boldsymbol{D},$ and $\boldsymbol{Q}$ fields. From this ANSYS can calculate the power output and the efficiency of the thermoelectric leg.

3. Methods

3.1. Temperature monitoring

Temperature data was collected from a steam trap at the UC Davis August A. Busch III Pilot Brewery. Temperatures were monitored using a Type-K thermocouple and data logger (Omega, Inc.) affixed to a steam trap pipe via Kapton tape. The temperature was measured every 15 s for one brewing cycle. Due to the thermal resistance resulting from this attachment method the data collected are a lower bound on T; fluid temperatures inside each manifold are expected to exceed surface temperatures. Temperatures were monitored for the duration of one brewing cycle. A representative subset of this data was used for power generation analysis. As can be seen from Fig. 2, the data contain short "cycles" where the temperature spikes up to some value and then decreases as a result of duty cycle-based steam heating of the system. The steam has a constant input temperature and duration and frequency of these heating cycles are varied to maintain the desired brewing temperature. The representative subset selected was from one of these "heating cycles" as it accurately represents the temperature variation as a function of time for a given brew cycle.

3.2. ANSYS modeling

Finite Element Modeling software ANSYS was used to formulate the model used to predict the power output. In addition to the Seebeck and Peltier effects, this thermal-electric analysis also accounts for Joule heating and the Thomson effect as a coupling mechanism between thermal and electric fields as mentioned previously [22]. This allows for an accurate and efficient analysis of thermoelectric materials. A steady-state analysis was performed using coupled-field elements SOLID226 and CIRCU124 to determine the power output (P), the thermal efficiency (η), and the electric current (I) of 4 different kinds of thermoelectric elements: (1) *Doped CoSb₃*,
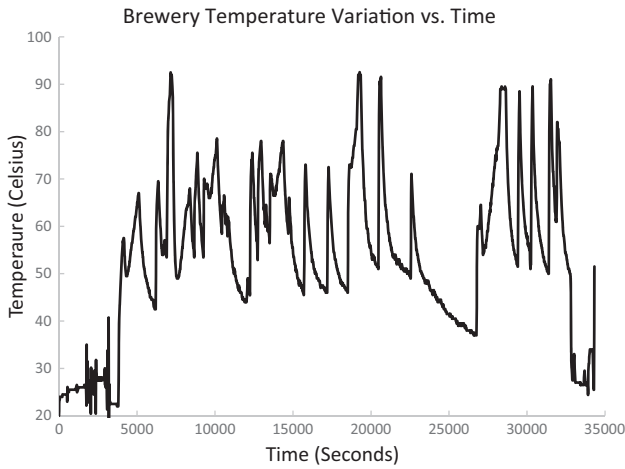
Fig. 2. Temperature variation with time measured at the UC Davis Pilot Brewery via a Type-K Thermocouple. The brew cycle shows characteristic spikes and drops in temperature as a function of time. The constant fluctuation in temperature appears to be a measure for controlling the brewing temperature. One of these characteristic sub-cycles was used as a sample input for further analysis.

Fig. 3. Schematic of the ANSYS Finite Element Model. As can be seen there is a temperature gradient that exists along the length of a thermoelement, with the two ends maintained at fixed temperatures. The blue end represents the cold junction while the red end represents the hot junction. Temperature variation is only considered along the axial direction.

[23] (2) $BiSbTe$ [24], (3) $SiGe$ [25], and (4) $Ti - doped(Zr, Hf)NiSn$ half-Heusler alloy [26]. These materials were selected because they represent the latest cutting-edge developments in research of thermoelectric materials. The analysis procedure consists of the following sub-steps:

1) Building the geometrical model of the thermoelectric couple based on L_{opt}, which represents the optimized leg length of a material with respect to power output.
2) Meshing the geometrical model.
3) Defining temperature dependent material properties and boundary conditions.
4) Constructing an electrical circuit and defining external resistance.
5) Solving using ANSYS APDL Mechanical Solver.

The model takes into account temperature-dependent material properties, namely thermal conductivity (λ), electrical conductivity (θ), and Seebeck coefficient (S). The power output depends on the hot side temperature (T_H), optimal leg lengths (L_{opt}) (obtained from LeBlanc et al.) [1–3], temperature-dependent material properties, and external resistance. ANSYS calculations were carried out using a constant cold-side temperature boundary condition of 22 °C and the hot-side temperature boundary conditions were determined from the real-time temperature measurements made at the UC Davis Pilot Brewery. The hot sides of the thermoelements were coupled in temperature and voltage while the cold sides were connected to an external resistance, and the analysis was performed under load-matched conditions to maximize the power output. At the cold junction, one thermoelement was specified to be the input electrical terminal, while the other thermoelement was set as the output electrical terminal (ground). Figure 3 shows schematic of the model developed using ANSYS Mechanical APDL.

3.3. Net present value and economic projections method

3.3.1. Costs

After calculating the expected power output from the 4 thermoelectric materials given the temperature conditions at the pilot brewery, an economic analysis was performed to assess the financial feasibility of a small-scale TEG installation. Power values were integrated into an economic mo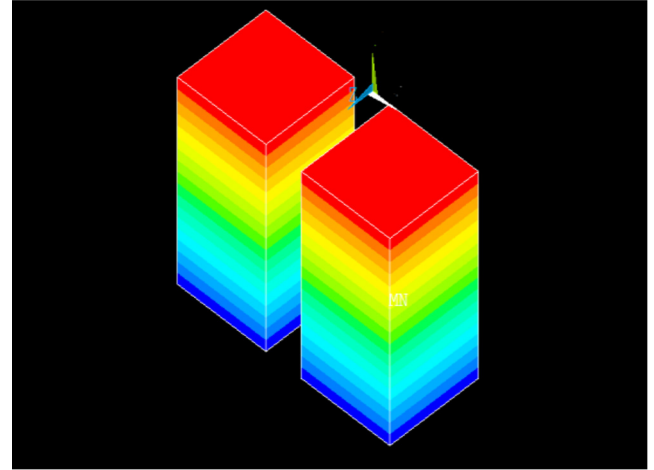del that accounted for costs and cash flows from both energy produced and carbon credits. Bulk material costs C_{bulk}, as well as optimal leg lengths L_{opt} and fill factors F were obtained from Leblanc et al. (Table 1). Manufacturing processes and total system cost components are evaluated to provide product development and commercial feasibility contexts [1–3] and module costs were calculated as the material-specific areal costs

$$C_{TEG}\left(\frac{\$}{m^2}\right): \ C_{TEG} = C_{bulk}^* \rho^* L^* F$$

Multiplied by the estimated area of the heat source. Heat exchanger areal cost was taken to be $\$18.48\left(\frac{W}{K}\right)^{-1}$ with a heat exchange coefficient U of $100\frac{W}{K}$, resulting in an area cost $C_{HX} = 1848\frac{\$}{m^2}$. Balance of system cost C_{BoS} and installation cost C_I were estimated as 10% each of the total areal cost: (see Table 2)

$$C_{BoS} = C_I = 0.1(C_{TEG} + C_{HX})$$

Resulting in a total capital cost $C_0 = (C_{TEG} + C_{HX} + C_{BoS} + C_I)$. Operation and maintenance cost may be safely neglected, as one major advantage of solid state TEG installations is the lack of necessary maintenance and upkeep after the initial installation [27]. System lifetime was taken as 25 years with a power degradation rate d of 1% per annum [27], and the system area was taken as 0.5 m².

3.3.2. Income

Incoming cash flows consist of the value of electricity purchases offset by TEG generation, C_e, as well as the value of any carbon credits for CO_2 generation offset by power produced from the TEG installation, C_{CO_2}. Electricity and carbon credit values are assumed to vary over time (Fig. 4), and the values used in this study are taken from the UC Davis prospectus on future energy planning [28]. Carbon offsets consistent with the current UC Davis energy purchase portfolio of 0.31 kg CO_2/kW h were used to calculate the value of carbon credit income streams. A discount rate r of 6% was assumed for all future cash flows consistent with UC Davis projections [28] and the total market average cost of capital [29]. Net present value is given by:

$$NPV = -C_0 + \sum_{i=0}^{T}\frac{C_e + C_{CO_2} + C_{O\&M}}{(1+r)^i(1+d)^i} \tag{9}$$

Table 1
Material and model parameters from Leblanc et al., and the resultant averaged real power output from the ANSYS model. Parameters are used in determining initial costs and lifetime power output.

Material	Bulk cost ($ /kg)	Density (kg/m³)	Optimal leg length (mm)	Optimal fill factor (F)	C_{TEG} ($ /m²)	Average power output (W/m²)
$CoSb_3$	24	7683	10.6	0.31	605	158
$BiSbTe$	125	6900	4.41	0.21	799	526
$SiGe$	679	4486	2.66	0.07	567	244
$(Zr, Hf) NiSn$	9.71	8296	19.6	0.49	942	115

Table 2
Areal power output and materials cost for 4 different material based TEGs, and net present value of the entire thermoelectric installation after 25 years of use based on average power output.

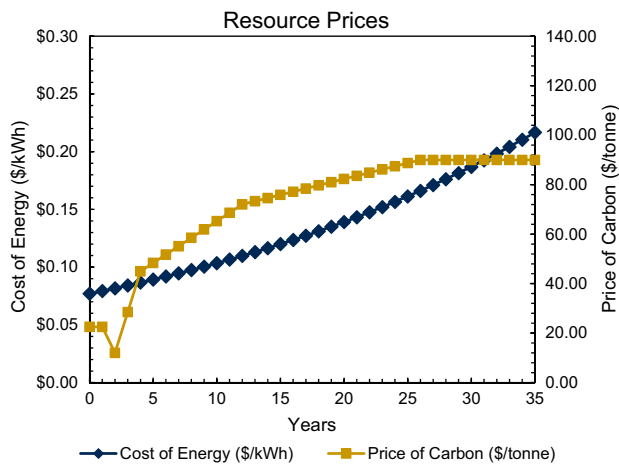| Material	Power (W/m²)	C_{TEG} ($/m²)	Net present value at 25 years ($)
$CoSb_3$	158	$ 605	−$ 461
$BiSbTe$	526	$ 798	$ 1777
$SiGe$	244	$ 567	$ 114
$(Zr, Hf)NiSn$	115	$ 773	−$ 834

Fig. 4. Cost of energy and price of carbon expected variation over the next 35 years.

where T is the predicted lifetime of the installation.

3.4. Estimation of parameters for seven-year payback

The power output $P(W/m^2)$ of a thermoelectric system is given as $P = \eta \cdot Q$, where η is the device efficiency and Q is the heat flux through the thermoelectric element:

$$Q = k\nabla T \tag{10}$$

Assuming a constant T_C of 22 °C and known thermal conductivity (k) and leg length (L_{opt}) corresponding to those of $SiGe$ above [2,25] the heat flux through the device was calculated in ANSYS for T_H ranging from 127 to 527 °C. The expected power outputs at these temperature ranges were then used to estimate parameter values that would enable a 7 year payback period.

The NPV model may be used to determine the necessary TEG power output at any given capital cost C_o that results in a payback period of no longer than 7 years. These calculated power outputs may be considered as a function of zT and T_H of an idealized TEG via Eqs. (2) and (3), thereby defining a surface in the parameter space of C_0, T_H, and zT that results in a seven-year payback period.

4. Results and discussion

4.1. Power output results from ANSYS model

In the plot below, the power density in W m^{-2} has been plotted as a function of the hot-side temperature for the 4 different thermoelectric materials.

The power output from a TE device depends on the zT, L_{opt}, and A_{TE} where L_{opt} is the optimal length for a given material to hold a temperature gradient, and A_{TE} is the cross-sectional area of the material. In this study, A_{TE} is taken to be the same for all materials, while L_{opt} values are obtained from [2]. A material with a high zT in a given temperature range and a low L_{opt} will have a high power out. $BiSbTe$ correspondingly gives the highest power output since it has the highest zT in the working temperature range and a very low L_{opt} [2]. The results shown in Fig. 5 nicely reflect this interplay between zT and L_{opt} to determine the power output. The power output results were compared and found to be consistent with experimental results from commercial TEG modules manufactured by HI-Z from similar TE materials, $BiSbTe$ in particular.

Using a Finite Element Modeling (FEM) software like ANSYS Mechanical APDL to model thermoelectric generators is an improvement over simplified analytical models that are used in literature [8]. These simplified models set up an overall thermal balance and assume a symmetrical distribution of the Joule effect between the hot and cold junctions [8]. These models may or may not factor in the Thomson effect and use material properties that have been evaluated at an average temperature of the two junctions: $(T_H + T_C)/2$. In order to accurately model thermoelectric devices, the Thomson effect and the non-linearity, which arises due to the temperature dependence of material properties, must be accounted for. This requires using a FEM software like ANSYS [8].
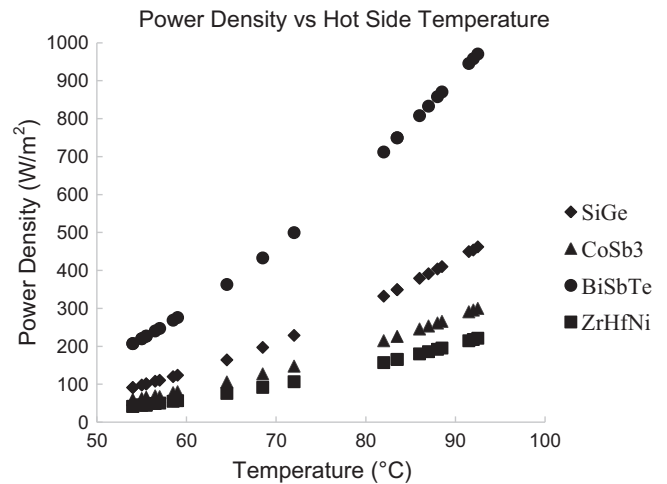

Fig. 5. Power output as a function of hot side temperature as calculated by ANSYS for four the different thermoelectric materials. $BiSbTe$ is predicted to generate the most electrical power given temperature conditions in this case study.

4.2. Net present value and parameter sensitivity results (25 years)

The results obtained from the economic analysis described in the methods sections are summarized in Table 1. It can be seen that the NPVs calculated at 25 years for two of the different materials are negative, one is near break-even, and one is significantly positive. The reason for this can be attributed primarily to the relatively low power outputs of $CoSb_3$ and $(Zr, Hf)NiSn$ in the low-temperature regime. Consistent with the power output values, BiSbTe has the highest NPV after 25 years. A low or negative NPV may nonetheless be justified in cases where power generation by other means is already expensive, or where power generation via heat recapture facilitates functionalities that would not otherwise be possible [4,6,11–13]. The baseline alternative to TEGs, traditional heat exchangers, must also be considered as an alternative. The utility of process heat, either recaptured for use in an industrial process or simply used as inexpensive area heating in climates requiring same, is highly dependent on the circumstances of its generation, and thus has value that is difficult to generalize. Many industrial processes are run continuously, which provides an opportunity for the recapture and re-use of process heat. However, in the case of a small brewery such as the system on which the temperature data used here was recorded, recaptured heat has little utility, and thus little value, unless the brewery is run in continuous operation—uncommon at the scale considered here. Where the value of process heat can be directly calculated, those results may be directly compared to the output of the modeling methodology presented here in order to make the optimal financial decision. In the broader context, this modeling methodology may be considered most appropriate for contexts in which traditional process heat recapture has been precluded by the circumstances of the installation.

Sensitivity analyses were performed on various aspects of the NPV model in order to determine factors, which play a dominant role in determining the financial viability of this technology. These analyses are based nominally on BiSbTe, with one variable at a time modified (Fig. 6): material cost (Fig. 6a), heat exchanger coefficient (Fig. 6b), discount rate (Fig. 6c), and power output (Fig. 6d). Comparison of Fig. 6a and b indicate that the system is more sensitive to changes in the heat exchanger cost than to material cost; this follows from the relative expense of the two components: at $U = 100$ (W/K) the heat exchanger in a BiSbTe-based TEG installation costs over twice as much as the active material. In such a scenario the dominant system cost is the heat exchanger, indicating the need for careful system design to minimize heat exchanger costs in low-temperature scenarios: such installations may be
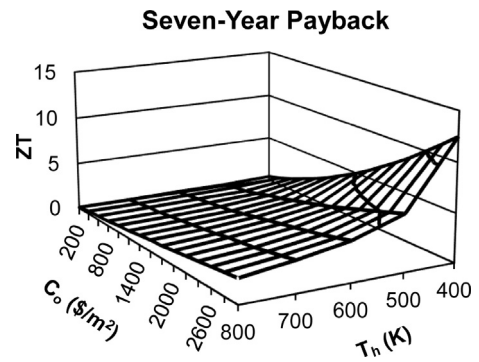

Fig. 7. The surface in cost-temperature-thermoelectric figure of merit zT space that defines the lower bound of parameters required for seven-year payback for a SiGe based TEG. Any point on or above this surface will provide a payback period of 7 years or less.
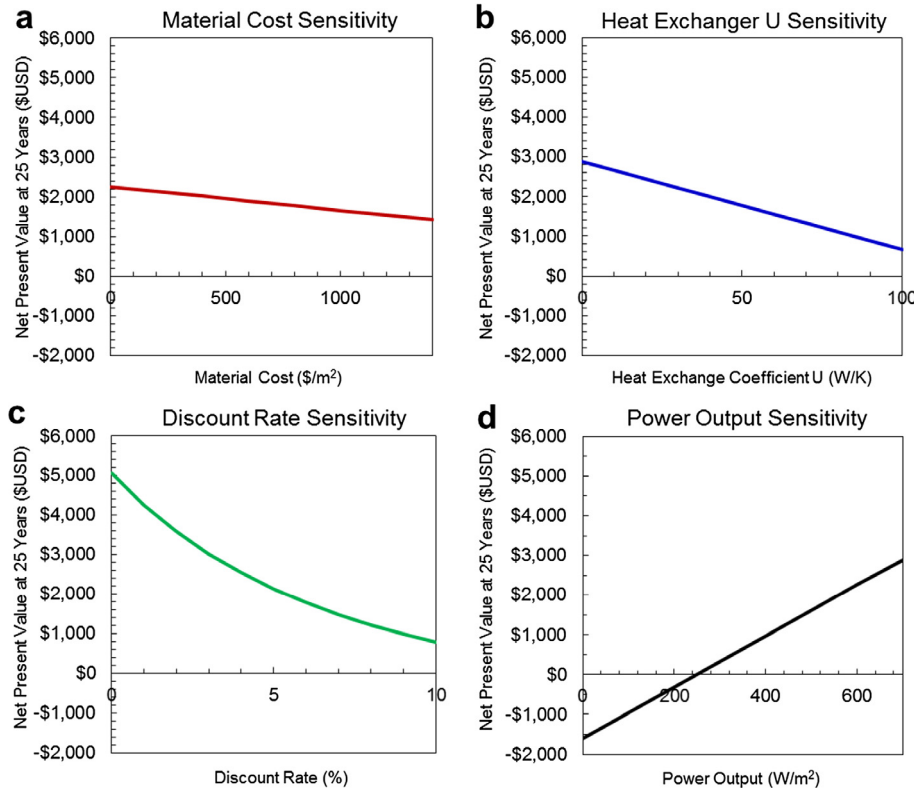

Fig. 6. Sensitivity analyses of the net present value with respect to material cost (a), heat exchanger U value (b), model discount rate (c), and power output (d). Plots show the necessary parameters for 25-year payback given the material transport and device design parameters of BiSbTe

feasible if passive air cooling is sufficient to maintain a stable T_H, or if existing heat exchanger infrastructure exists and may be inexpensively expanded.

At low temperatures less robust heat exchangers may suffice in providing sufficient heat removal at the TEG's cold side. For comparison a U between 40 and 50 W/K is comparable to simple heat exchange via atmospheric convection [30]. Such circumstances may be plausible for existing low-temperature heat sources that are situated in well-ventilated areas.

The financial circumstances of the party funding an installation may also be highly relevant to the economic feasibility of an installation by way of the discount rate assumed for the NPV model. The weight-adjusted cost of capital (WACC) accounts for the average cost of holding debt or equity for a given industry; that is, the rate of return expected from invested equity or the rate of interest paid on debt. This rate is commonly used as the discount rate when performing NPV calculations. The WACC for various industries ranges from 4% to 11% per annum; Fig. 6c shows the dependence of NPV on discount rate. In an installation such as this all capital outlays occur at year zero and all income occurs in future years, and is subject to discounting. Such an installation is therefore particularly sensitive to the choice of discount rate; therefore the same investment may be profitable for a business with low WACC, but less advisable for an industry with a higher WACC.

Finally the power output of an installation must be given consideration. The power output of an installation may be increased either by increasing the efficiency of the TEG used, or by increasing the temperature of the heat source. In either case, Fig. 6d indicates that a power output density of 250 W/m^2 is necessary for this installation to break even after 25 years, which at the given price point is achievable by *BiSbTe*-based TEGs, even with a low-temperature heat source such as the one considered here. Different materials are optimal for different temperature ranges, and thus the correct choice of material will be highly dependent on the prevalent thermal conditions. The *zT* of *BiSbTe* drops significantly above 100 °C, with *CoSb*3 demonstrating superior performance up to approximately 700 °C and *SiGe* performing well up to and above 1000 °C [21]. At these elevated temperatures a power density of 250 W/m^2 is feasible even with inefficient TEGs, though the problem of efficient cold-side heat exchange becomes significant.

4.3. Estimation of parameters for achieving seven-year payback results

The previous sensitivity analyses raise an important question: what combinations of device efficiency and heat source temperature are necessary to make any given TEG installation financially feasible? Many capital projects are considered infeasible if their payback period exceeds seven years. As such it is worthwhile to consider the interplay between capital cost, heat source temperature, and thermoelectric figure of merit that would provide a payback period of seven years. The NPV model may be used to calculate the necessary power output of a thermoelectric system at a given overall capital cost that achieves this payback period, which is possible if the system cost of power is below approximately \$5.30/W.

Determining the heat flux through the TEG at a given T_H and T_C is necessary for determining the device efficiency, and thus *zT*, required in order to produce the above power outputs. These heat fluxes $Q(T_H)$ were calculated in ANSYS given the same experimental parameters L_{opt} and k for *SiGe*. Based on these assumptions, Fig. 7 shows the parameter space of overall capital cost C_o, hot-side temperature T_H and device figure of merit *zT* necessary for achieving seven-year payback:

For high costs and low T_H, necessary *zT* values become prohibitively large. While *zT* values exceeding 2 have been

demonstrated at the laboratory scale, *zT* above 4 are an ambitious target for future technologies, with *zT*s in excess of 20 generally considered to be infeasible [31].

5. Conclusion

A method for predicting the power output and financial feasibility of a thermoelectric generator was devised using ANSYS finite-element software and experimental temperature measurements. The method accounts for temperature-dependent, experimentally determined materials properties and variable heat sources, providing a more robust predictive capability than simpler methods. The outputs of the ANSYS model were then used in a net present value model to calculate the financial feasibility of an installation based on a low-temperature heat source and four different leading candidate thermoelectric materials. Sensitivity analyses demonstrate that improvements may be made most effectively by identifying higher temperature heat sources, optimizing the choice of heat exchanger to eliminate excess costs, and identifying industries for investment with lower cost of capital. The use of TEGs may additionally facilitate added functionality that would not be possible without their use: for instance, in self-powered furnaces and co-generation systems [4–6] for use in remote regions, or for wearable electronics that may be powered indefinitely by harvesting body heat [11]. This methodology, along with its results, provides a powerful platform for analyzing the performance of real-world TEG systems, a strong predictive capability for financial analysis of potential applications, and useful context for where further technological development on TEG materials and devices would be most effective.

References

[1] LeBlanc S. Thermoelectric generators: linking material properties and systems engineering for waste heat recovery applications. Sustain Mater Technol 2014;1–2:26–35. http://dx.doi.org/10.1016/j.susmat.2014.11.002.

[2] LeBlanc S, Yee SK, Scullin ML, Dames C, Goodson KE. Material and manufacturing cost considerations for thermoelectrics. Renew Sustain Energy Rev 2014;32:313–27. http://dx.doi.org/10.1016/j.rser.2013.12.030.

[3] Yee SK, LeBlanc S, Goodson KE, Dames C. \$ per W metrics for thermoelectric power generation: beyond ZT. Energy Environ Sci 2013;6:2561–71. http://dx.doi.org/10.1039/C3EE41504J.

[4] Omer SA, Infield DG. Design and thermal analysis of a two stage solar concentrator for combined heat and thermoelectric power generation. Energy Convers Manage 2000;41:737–56. http://dx.doi.org/10.1016/S0196-8904(99)00134-X.

[5] Qiu K, Hayden ACS. Integrated thermoelectric generator and application to self-powered heating systems. In: 25th int conf thermoelectr 2006 ICT 06, 2006. p. 198–203. doi: http://dx.doi.org/10.1109/ICT.2006.331332.

[6] Abdul-Wahab SA, Elkamel A, Al-Damkhi AM, Al-Habsi IA, Al-Rubai'ey' HS, Al-Battashi AK, et al. Design and experimental investigation of portable solar thermoelectric refrigerator. Renew Energy 2009;34:30–4. http://dx.doi.org/10.1016/j.renene.2008.04.026.

[7] Montecucco A, Siviter J, Knox AR. Combined heat and power system for stoves with thermoelectric generators. Appl Energy 2015. http://dx.doi.org/10.1016/j.apenergy.2015.10.132.

[8] Kumar S, Heister SD, Xu XF, Salvador JR, Meisner GP. Thermoelectric generators for automotive waste heat recovery systems Part I: numerical modeling and baseline model analysis. J Electron Mater 2013;42:665–74. http://dx.doi.org/10.1007/s11664-013-2471-9.

[9] Wang YC, Dai CS, Wang SX. Theoretical analysis of a thermoelectric generator using exhaust gas of vehicles as heat source. Appl Energy 2013;112:1171–80. http://dx.doi.org/10.1016/j.apenergy.2013.01.018.

[10] Luo Y, Zhang L, Liu Z, Wang Y, Meng F, Wu J. Thermal performance evaluation of an active building integrated photovoltaic thermoelectric wall system. Appl Energy 2016;177:25–39. http://dx.doi.org/10.1016/j.apenergy.2016.05.087.

[11] Kim SJ, We JH, Cho BJ. A wearable thermoelectric generator fabricated on a glass fabric. Energy Environ Sci 2014;7:1959–65. http://dx.doi.org/10.1039/C4EE00242C.

[12] Hyland M, Hunter H, Liu J, Veety E, Vashaee D. Wearable thermoelectric generators for human body heat harvesting. Appl Energy 2016;182:518–24. http://dx.doi.org/10.1016/j.apenergy.2016.08.150.

[13] Lu Z, Zhang H, Mao C, Li CM. Silk fabric-based wearable thermoelectric generator for energy harvesting from the human body. Appl Energy 2016;164:57–63. http://dx.doi.org/10.1016/j.apenergy.2015.11.038.

[14] Liu D, Zhao FY, Yang HX, Tang GF. Theoretical and experimental investigations of thermoelectric heating system with multiple ventilation channels. Appl Energy 2015;159:458–68.

[15] Rezania A, Rosendahl LA. Feasibility and parametric evaluation of hybrid concentrated photovoltaic-thermoelectric system. Appl Energy 2017;187:380–9.

[16] Ding LC, Akbarzadeh A, Date A. Electric power generation via plate type power generation unit from solar pond using thermoelectric cells. Appl Energy 2016;183:61–76.

[17] Liu D, Zhao FY, Yang HX, Tang GF. Thermoelectric mini cooler coupled with micro thermosiphon for CPU cooling system. Energy 2015;83:29–36.

[18] (a) Hyland H, Hunter H, Liu J, Veety E, Vashaee D. Wearable thermoelectric generators for human body heat harvesting. Appl Energy 2016;182:518–24; (b) Fraisse G, Ramousse J, Sgorlon D, Goupil C. Comparison of different modeling approaches for thermoelectric elements. Energy Convers Manage 2013;65:351–6. http://dx.doi.org/10.1016/j.enconman.2012.08.022.

[19] Zhang T. New thinking on modeling of thermoelectric devices. Appl Energy 2016;168:65–74. http://dx.doi.org/10.1016/j.apenergy.2016.01.057.

[20] Högblom O, Andersson R. A simulation framework for prediction of thermoelectric generator system performance. Appl Energy 2016;180:472–82. http://dx.doi.org/10.1016/j.apenergy.2016.08.019.

[21] Snyder GJ, Toberer ES. Complex thermoelectric materials. Nat Mater 2008;7:105–14. http://dx.doi.org/10.1038/nmat2090.

[22] Antonova EE, Looman DC. Finite elements for thermoelectric device analysis in ANSYS. In: ICT 2005 24th int conf thermoelectr; 2005. p. 200–3. doi: http://dx.doi.org/10.1109/Ict.2005.1519922.

[23] Peng J, He J, Alboni PN, Tritt TM. Synthesis and thermoelectric properties of the double-filled Skutterudite Yb0.2In y Co4Sb12. J Electron Mater 2009;38:981–4. http://dx.doi.org/10.1007/s11664-008-0624-z.

[24] Xie W, Tang X, Yan Y, Zhang Q, Tritt TM. High thermoelectric performance BiSbTe alloy with unique low-dimensional structure. J Appl Phys 2009;105:113713. http://dx.doi.org/10.1063/1.3143104.

[25] Wang XW, Lee H, Lan YC, Zhu GH, Joshi G, Wang DZ, et al. Enhanced thermoelectric figure of merit in nanostructured n-type silicon germanium bulk alloy. Appl Phys Lett 2008;93:193121. http://dx.doi.org/10.1063/1.3027060.

[26] Sakurada S, Shutoh N. Effect of Ti substitution on the thermoelectric properties of (Zr, Hf)NiSn half-Heusler compounds. Appl Phys Lett 2005;86:082105. http://dx.doi.org/10.1063/1.1868063.

[27] Ferrotec (USA) corporation. Thermoelectric technical reference — reliability of thermoelectic coolers n.d.

[28] BmcD Engineering Company Inc, FvD Energy, Inc., Report on the campus heating & cooling systems: energy planning; 2014.

[29] Damodaran A. Cost of capital by sector (US); 2016.

[30] Kakaç S, Liu H, Pramuanjaroenkij A. Heat exchangers: selection, rating, and thermal design, third edition. 3rd ed. Boca Raton, FL: CRC Press; 2012.

[31] Vining CB. An inconvenient truth about thermoelectrics. Nat Mater 2009;8:83–5. http://dx.doi.org/10.1038/nmat2361.